Journal of Materials Chemistry

Cite this: *J. Mater. Chem.*, 2012, **22**, 5020

www.rsc.org/materials

PAPER

Mixed polymeric micelles as multifunctional scaffold for combined magnetic resonance imaging contrast enhancement and targeted chemotherapeutic drug delivery†

Tao Liu,[a] Yinfeng Qian,*[b] Xianglong Hu,[a] Zhishen Ge*[a] and Shiyong Liu*[a]

Received 9th October 2011, Accepted 12th January 2012
DOI: 10.1039/c2jm15092a

We report on the utilization of mixed diblock copolymer micelles as an integrated multifunctional platform for the cancer cell-targeted delivery of chemotherapeutic drugs and magnetic resonance (MR) imaging contrast enhancement under *in vitro* and *in vivo* conditions. Two types of amphiphilic diblock copolymers, PCL-*b*-P(OEGMA-FA) and PCL-*b*-P(OEGMA-*Gd*), consisting of a hydrophobic poly(ε-caprolactone) (PCL) block and a hydrophilic poly(oligo(ethylene glycol) monomethyl ether methacrylate) (POEGMA) block, covalently attached with folic acid (FA) and DOTA-Gd (Gd) moieties, respectively, were synthesized *via* the combination of atom transfer radical polymerization (ATRP), ring-opening polymerization (ROP), and "click" post-functionalization. Mixed micelles co-assembled from PCL-*b*-P(OEGMA-FA) and PCL-*b*-P(OEGMA-Gd) possess hydrophobic PCL cores for loading chemotherapeutic drugs and hydrophilic POEGMA outer coronas functionalized with FA and Gd complexes for synergistic functions of targeted delivery and MR imaging contrast enhancement. As-prepared nanosized mixed micelles are capable of physically encapsulating paclitaxel, a well-known hydrophobic anticancer drug, with a loading content of ~5.0 w/w%, exhibiting controlled release of up to ~60% loaded drugs over a duration of ~130 h. *In vitro* cell viability assays revealed that drug-free mixed micelles are almost non-cytotoxic up to a concentration of 0.2 g L^{-1}, whereas paclitaxel-loaded ones can effectively kill HeLa cells at the same concentration. *In vitro* MR imaging experiments indicated dramatically increased T_1 relaxivity (26.29 s^{-1} mM^{-1}) for mixed micelles compared to that of small molecule counterpart, alkynyl-DOTA-Gd (3.12 s^{-1} mM^{-1}). Further *in vivo* MR imaging experiments in rabbits revealed considerably enhanced signal intensity, prominent positive contrast enhancement, improved accumulation and retention, and extended blood circulation duration for FA-labeled mixed micellar nanoparticles within the rabbit liver, as compared to those for FA-free mixed micelles and small molecule alkynyl-DOTA-Gd complex. These preliminary results indicate that the reported mixed micellar nanocarriers possess synergistically integrated functions of cancer-targeted drug delivery and controlled release, and MR imaging contrast enhancement, which augurs well for their potential application as a novel type of theranostic platform.

1. Introduction

Chemotherapy has been well-recognized as a major cancer therapeutic modality for the post-surgery period, providing promising opportunities for overcoming cancer heterogeneity and adaptation concerns. To solve the intrinsic limitations associated with small molecule cancer chemotherapeutic drugs, such as poor water solubility, unsatisfactory pharmacokinetic processes, and severe side effects, new strategies have been developed by physically encapsulating or covalently functionalizing small molecule drugs onto polymer scaffolds and polymeric assemblies (*e.g.*, micelles and vesicles) to achieve enhanced water solubility, improved loading capacity, sustained controlled release or on-demand triggered release, specific accumulation within tumor tissues, and prolonged *in vivo* circulation duration.[1–6]

On the other hand, the integration of controlled-release polymeric drug nanocarriers with detection and diagnostic functions proves to be another promising direction.[7,8] The so-called theranostic nanomedicines are capable of combined functions such as

[a]*CAS Key Laboratory of Soft Matter Chemistry, Hefei National Laboratory for Physical Sciences at the Microscale, Department of Polymer Science and Engineering, University of Science and Technology of China, Hefei, Anhui, 230026, China. E-mail: sliu@ustc.edu.cn; liangminqyf@sohu.com; gezs@mail.ustc.edu.cn*
[b]*The First Affiliated Hospital of Anhui Medical University, Hefei, Anhui, 230022, China*

† Electronic supplementary information (ESI) available: Supplementary figs. S1–S3. See DOI: 10.1039/c2jm15092a

chemotherapy, and the monitoring of pathological progress and therapeutic efficacy.[9–17] For clinical disease detection and diagnosis applications, the magnetic resonance (MR) imaging technique has emerged to be one of the most powerful choices, which offers advantages such as high spatiotemporal resolution, no exposure to radiation, noninvasiveness, excellent penetration depths, and high sensitivity towards soft tissues.[18,19] Typical contrast agents include T_1-type Gd complexes (*e.g.*, DOTA-Gd and DTPA-Gd)[20–26] and T_2-type ones such as superparamagnetic iron oxide (SPIO) nanoparticles[27–33] and $MnFe_2O_4$ nanoparticles.[34,35] Future developments in the field of MR imaging contrast agents rely on the screening of more efficient ones with higher relaxivity, their combination with other diagnostic techniques (*e.g.*, PET, CT, fluorescence), and the integration with therapeutic functions such as drug and gene delivery.[18,36–40]

In addition, micelles and vesicles self-assembled from amphiphilic diblock copolymers have been under in-depth scrutiny for their applications as nanocarriers for chemotherapeutic drugs.[5,6] Note that polymeric assemblies also prove to be an excellent platform for the construction of a new generation of theranostic nanomedicines.[41] It can be envisaged that the integration of drug delivery and controlled release functions with MR imaging enhancement capabilities will endow the theranostic ensemble with combined advantages such as excellent water dispersibility, *in vivo* biocompatibility, and enhanced MR imaging performances, due to the specific accumulation of nanoassemblies within tumor tissues *via* the enhanced permeability and retention (EPR) effect.[14] In this context, several research groups have contributed to the field of polymeric assembly-based theranostic systems integrated with the functions of targeted drug delivery/controlled release and MR imaging enhancement, and focusing on polymeric micelles or vesicles encapsulating T_2-type SPIO nanoparticles.[32,33,35,42–51]

Although T_1-type MR imaging contrast agents such as the DTPA-Gd complex are quite frequently used in clinical disease diagnosis due to the fact that they provide favorably positive contrast enhancement, compared to the T_2-type ones described above, the integration of a small molecule Gd complex-based contrast agent with polymeric assemblies has been far less explored.[18,52–56] There exist several relevant reports concerning this aspect.[52–55,57] Wooley *et al.*[57] attached a DTPA-Gd complex onto the hydrophilic corona of shell cross-linked micelles of a poly(methyl acrylate)-*b*-poly(acrylic acid) diblock copolymer (PMA-*b*-PAA). This resulted in a ~9-fold increase in T_1 relaxivity (r_1) compared to small molecule Gd complexes. Li *et al.*[53] functionalized hydrophilic coronas of poly(lactic acid)-*b*-poly(L-glutamic acid) (PLA-*b*-PGA) diblock copolymer micelles with a DTPA-Gd complex, and a ~2-fold increase in r_1 was observed.

In the above examples, the cancer cell-targeted delivery function cannot be achieved due to the lack of targeting moieties in the nanocarrier design. We recently reported on the fabrication of multifunctional polymeric unimolecular micelles possessing hyperbranched polyester cores, hydrophobic PCL inner layers, and hydrophilic outer coronas, covalently labeled with a DOTA-Gd (Gd) complex and folic acid (FA) targeting functionalities.[58] Besides acting as targeted drug delivery nanocarriers, the as-prepared unimolecular micelles exhibit a ~5.8-fold increase in r_1 compared to the small molecule Gd complex. However, the synthesis of the above-mentioned unimolecular micelles involves the click functionalization of two types of reagents (for MR imaging contrast enhancement and cancer cell targeting, respectively) onto the polymeric scaffold, which is quite tedious and difficult to control and quantify accurately.

For polymeric micelle-based theranostic nanomedicine involving MR imaging and targeted drug delivery functions, the grafting density and surface distribution of contrast agents (*e.g.*, Gd complex) and targeting moieties (*e.g.*, FA), and their relative ratios within the corona layer of the micelles will affect the cancer chemotherapeutic efficacy and MR imaging contrast performance.[4,6,33] The screening of an effective theranostic system will typically involve fine tuning of the above parameters. In the past few years, mixed micelles assembled from two or more types of dissimilar diblock copolymers with varying chemical compositions, block length ratios, and functionalities have emerged to be a new type of design platform for drug delivery nanocarriers.[5,6] They typically offer advantages such as improved physical stability, enhanced drug loading capacity, and most importantly, the integration of multiple functions into a single system, as summarized by Yang *et al.*[6] in a recent review article.

We then envisaged that mixed micelles self-assembled from two types of amphiphilic diblock copolymers, respectively labeled with a small molecule T_1-type contrast agent (Gd complex) and targeting functionalities (FA) might be capable of solving the limitations described in the previous section. Herein, we report on the utilization of mixed diblock copolymer micelles as an integrated multifunctional platform for the cancer cell-targeted delivery of chemotherapeutic drugs and MR imaging contrast enhancement under *in vitro* and *in vivo* conditions (Scheme 1). Two types of amphiphilic diblock copolymers, PCL-*b*-P(OEGMA-FA) and PCL-*b*-P(OEGMA-Gd), consisting of hydrophobic PCL and hydrophilic poly(oligo(ethylene glycol) monomethyl ether methacrylate) (POEGMA) covalently attached with FA and DOTA-Gd (Gd) moieties, respectively, were synthesized at first, *via* the combination of atom transfer radical polymerization (ATRP), ring-opening polymerization (ROP), and "click" post-functionalization (Scheme 2). Mixed micelles co-assembled from PCL-*b*-P(OEGMA-FA) and PCL-*b*-P(OEGMA-Gd) possess a hydrophobic PCL core for the loading

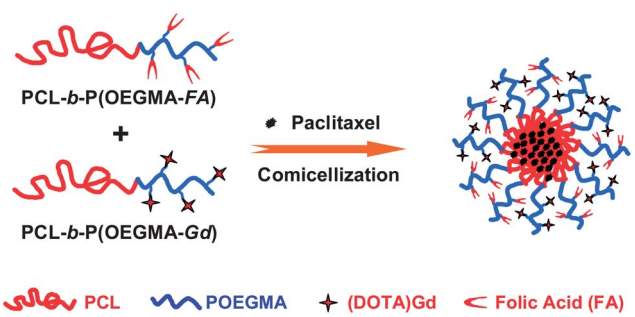

Scheme 1 Schematic illustration of the fabrication of tumor-targeted polymeric micelles *via* the co-assembly of two amphiphilic diblock copolymers, PCL-*b*-P(OEGMA-Gd) and PCL-*b*-P(OEGMA-FA), in aqueous solution. The mixed micelles consist of PCL as the hydrophobic core and a hydrophilic outer corona of POEGMA covalently labeled with folic acid (FA) and DOTA-Gd (Gd) for synergistic targeted drug delivery and MR imaging.

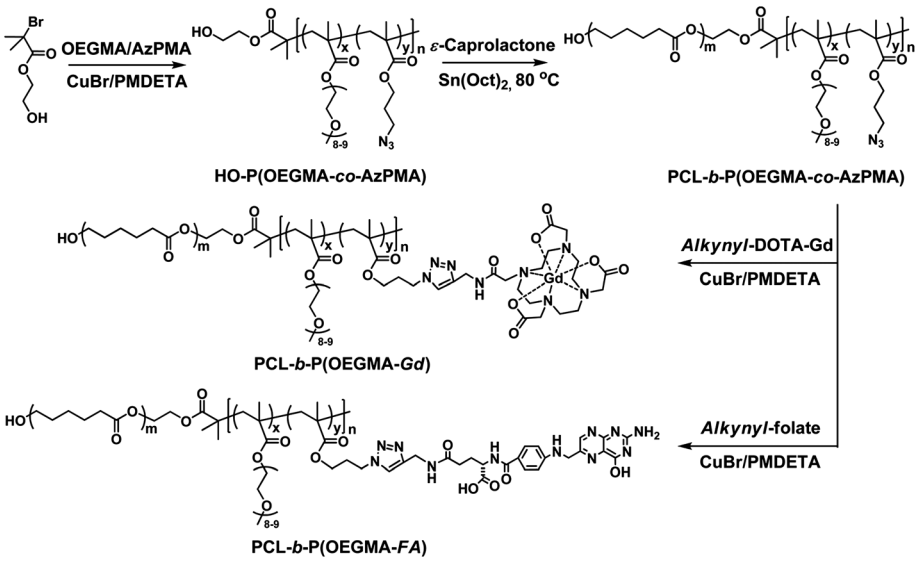

Scheme 2 Synthetic schemes employed for the preparation of the well-defined amphiphilic diblock copolymers, PCL-*b*-P(OEGMA-Gd) and PCL-*b*-P(OEGMA-FA), covalently attached with T_1 weighted MR imaging contrast agents (DOTA-Gd, Gd) and tumor-targeting moieties, folic acid (FA), respectively, in the hydrophilic POEGMA block.

of chemotherapeutic drugs and a hydrophilic outer corona of POEGMA functionalized with FA and DOTA-Gd (Gd) for synergistic targeted drug delivery and MR imaging contrast enhancement. *In vitro* and *in vivo* MR imaging tests, *in vitro* drug release profiles, and cytotoxicity measurements of drug-free and drug-loaded mixed micelles were conducted to probe the feasibilities and capabilities of this new type of mixed micelle-based theranostic system.

2. Experimental

Materials

Oligo(ethylene glycol) monomethyl ether methacrylate (OEGMA, M_n = 475 g mol^{-1}, mean degree of polymerization, DP, is 8–9) purchased from Aldrich was passed through a neutral alumina column to remove the inhibitor and then stored at −20 °C prior to use. ε-Caprolactone (CL, 99%, Acros) was dried over calcium hydride (CaH_2) and distilled at reduced pressure before use. *N*,*N*,*N*′,*N*″,*N*″-Pentamethyldiethylenetriamine (PMDETA, 98%), copper(I) bromide (CuBr, 98%), stannous(II) octanoate ($Sn(Oct)_2$, 95%), and paclitaxel were purchased from Aldrich and used as received. Fetal bovine serum (FBS), penicillin, streptomycin, and Dulbecco's modified Eagle's medium (DMEM) were purchased from GIBCO and used as received. Toluene was dried by refluxing over sodium shavings and distilled just prior to use. Isopropanol (IPA), tetrahydrofuran (THF), dimethylformamide (DMF), and all other reagents were purchased from Sinopharm Chemical Reagent Co. Ltd. and used as received. Water was deionized with a Milli-Q SP reagent water system (Millipore) to a specific resistivity of 18.4 MΩ cm. 2-Hydroxyethyl 2-bromo-2-methylpropanoate (HBMP),[59] 3-azidopropyl methacrylate (AzPMA), alkynyl-functionalized folic acid, alkynyl-folate,[60] and alkynyl-functionalized DOTA-Gd complex, alkynyl-DOTA-Gd (DOTA: 1,4,7,10-tetraazacyclododecane-1,4,7,10-tetrakisacetic acid)[61,62] were synthesized according to the literature procedures.

Sample preparation

The synthetic routes employed for the preparation of amphiphilic diblock copolymers, PCL-*b*-P(OEGMA-Gd) and PCL-*b*-P(OEGMA-FA), are shown in Scheme 2.

Synthesis of P(OEGMA-*co*-AzPMA). HBMP (0.32 g, 1.52 mmol), OEGMA (21.66 g, 45.6 mmol), AzPMA (1.28 g, 7.6 mmol), PMDETA (0.26 g, 1.52 mmol), and isopropanol (25 mL) were charged into a reaction flask. The mixture was degassed by three freeze–pump–thaw cycles and backfilled with nitrogen. After heating to 35 °C, CuBr (0.22 g, 1.52 mmol) was introduced as a solid under the protection of N_2 to start the polymerization. After stirring for 3 h, the reaction tube was quenched into liquid N_2, opened and exposed to air, and diluted with 30 mL THF. The mixture was then passed through a silica gel column using THF as the eluent to remove the copper catalysts. After removing all the solvents on a rotary evaporator, the residues were dissolved in THF and precipitated into an excess of cold *n*-hexane. The above dissolution–precipitation cycle was repeated three times. The final product was dried in a vacuum oven overnight at room temperature, yielding a white viscous solid (10.6 g, yield: 45.7%). The molecular weight and molecular weight distribution of P(OEGMA-*co*-AzPMA) were determined by GPC using THF as the eluent, revealing an M_n of 8000 and a M_w/M_n of 1.13 (Fig. 1a). The conversion of OEGMA and AzPMA were determined to be 49.8% and 61.2%, respectively, based on ^{1}H NMR analysis of the crude product before purification. Due to the overlapping of resonance signals characteristic of OEGMA and AzPMA residues within the final polymer, this represents the best estimation of the relative contents of two co-monomers within the copolymer. In combination with the M_n data determined

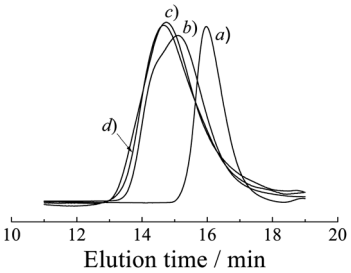

Fig. 1 THF GPC traces recorded for (a) P(OEGMA$_{0.83}$-*co*-AzPMA$_{0.17}$)$_{18}$, (b) PCL$_{64}$-*b*-P(OEGMA$_{0.83}$-*co*-AzPMA$_{0.17}$)$_{18}$, (c) PCL-*b*-P(OEGMA-Gd), and (d) PCL-*b*-P(OEGMA-FA).

from GPC, the chemical structure of the product was determined to be P(OEGMA$_{0.83}$-*co*-AzPMA$_{0.17}$)$_{18}$.

Synthesis of PCL-*b*-P(OEGMA-*co*-AzPMA) amphiphilic diblock copolymers. PCL-*b*-P(OEGMA-*co*-AzPMA) was synthesized *via* the ROP of CL using P(OEGMA$_{0.83}$-*co*-AzPMA$_{0.17}$)$_{18}$ as the macroinitiator. P(OEGMA$_{0.83}$-*co*-AzPMA$_{0.17}$)$_{18}$ (2.28 g, 0.3 mmol), CL (3.42 g, 30 mmol), and dry toluene (15 mL) were charged into a glass ampoule equipped with a magnetic stirring bar. About 5 mL toluene was removed under reduced pressure at first. Then a 1.5 mL solution of Sn(Oct)$_2$ in toluene (0.1 mol L^{-1}) was added under nitrogen protection. After removing another ~5 mL toluene under reduced pressure, the glass ampoule was carefully sealed under vacuum and stirred at 70 °C for 12 h. The reaction tube was quenched into liquid N_2, exposed to air, diluted with THF, and precipitated into an excess of diethyl ether–*n*-hexane (1 : 2, v/v). The above dissolution–precipitation cycle was repeated three times. The final product was dried in a vacuum oven overnight at room temperature to afford a white solid (4.4 g, yield: 77.2%). The molecular weight and molecular weight distribution of PCL-*b*-P(OEGMA-*co*-AzPMA) were determined by GPC using THF as the eluent, revealing an M_n of 15 600 and a M_w/M_n of 1.39 (Fig. 1b). The DP of the PCL block was determined to be 64 by ^{1}H NMR analysis in $CDCl_3$ (Fig. S1a, ESI†). Thus, the polymer was denoted as PCL$_{64}$-*b*-P(OEGMA$_{0.83}$-*co*-AzPMA$_{0.17}$)$_{18}$ and shortened as PCL-*b*-P(OEGMA-*AzPMA*) in subsequent sections.

Synthesis of PCL-*b*-P(OEGMA-FA) and PCL-*b*-P(OEGMA-Gd) amphiphilic diblock copolymers. Amphiphilic diblock copolymers, PCL-*b*-P(OEGMA-FA) and PCL-*b*-P(OEGMA-Gd), were obtained by the click reaction of PCL$_{64}$-*b*-P(OEGMA$_{0.83}$-*co*-AzPMA$_{0.17}$)$_{18}$ precursor with alkynyl-folate and alkynyl-DOTA-Gd, respectively. PCL$_{64}$-*b*-P(OEGMA$_{0.83}$-*co*-AzPMA$_{0.17}$)$_{18}$ (1.49 g, 0.10 mmol azide moieties), alkynyl-folate (0.20 g, 0.42 mmol), PMDETA (17 mg, 0.10 mmol), and DMF (10 mL) were charged into a glass ampoule equipped with a magnetic stirring bar. The mixture was degassed by three freeze–pump–thaw cycles, and then CuBr (14 mg, 0.10 mmol) was introduced under nitrogen. After thermostatting at 60 °C in an oil bath and stirring for 12 h, the reaction tube was quenched into liquid N_2, opened and exposed to air, and diluted with 30 mL THF. The reaction mixture was then passed through a basic alumina column using THF as the eluent to remove the copper catalysts. After removal of all the solvents on a rotary evaporator, the residues were dissolved in THF and precipitated into an excess of cold *n*-hexane. The obtained white solid was further purified by dialysis (cellulose membrane, molecular weight cutoff: 3500 Da) against deionized water for 12 h, and then lyophilized as a white solid (1.51 g, yield: 89.3%). GPC characterization revealed an M_n of 16 500 and a M_w/M_n of 1.38 (Fig. 1d). UV–vis analysis in DMSO using folic acid as the calibration standard indicated the quantitative transformation of azide groups to folate moieties. Thus, the polymer was denoted as PCL$_{64}$-*b*-P(OEGMA$_{0.83}$-*co*-FA$_{0.17}$)$_{18}$ and shortened as PCL-*b*-P(OEGMA-FA). By employing similar protocols, an amphiphilic diblock copolymer covalently labeled with DOTA-Gd complex in the POEGMA block was also synthesized. GPC analysis revealed an M_n of 16 700 and a M_w/M_n of 1.39 (Fig. 1c). The Gd^{3+} content within the diblock copolymer was determined to be ~2.8 wt% by inductively coupled plasma atomic emission spectrometry (ICP–AES) measurements. Thus the polymer was denoted as PCL$_{64}$-*b*-P(OEGMA$_{0.83}$-*co*-Gd$_{0.17}$)$_{18}$ and shortened as PCL-*b*-P(OEGMA-Gd).

Fabrication of mixed diblock copolymer micelles. Mixed micelles co-assembled from PCL-*b*-P(OEGMA-Gd) and PCL-*b*-P(OEGMA-FA) were prepared *via* the common solvent approach. In a typical example, PCL-*b*-P(OEGMA-Gd) and PCL-*b*-P(OEGMA-FA) (1 : 1, wt/wt) were dissolved in DMF. Then the polymer solution was dialyzed directly against deionized water for 24 h (cellulose membrane, molecular weight cutoff, MWCO, is 3500 Da), fresh deionized water was replaced every 6 h. Finally, the colloidal dispersion was diluted to the desired concentrations for further experiments.

Preparation of paclitaxel-loaded mixed micelles. Typical procedures employed for the encapsulation of paclitaxel into mixed polymeric micelles are as follows. PCL-*b*-P(OEGMA-Gd) (5.0 mg), PCL-*b*-P(OEGMA-FA) (5.0 mg), and paclitaxel (1.0 mg) were dissolved in 2.0 mL THF. Then 8.0 mL deionized water was added dropwise into the solution under vigorous stirring over ~1 h. The mixture was stirred at 50 °C to remove organic solvents. Unsolubilized paclitaxel was removed by passing it through 0.45 μm Millipore Acrodisc-12 filters. The micellar solution was diluted with deionized water to 9.0 mL and then with phosphate buffer solution (PBS; 0.2 M, pH 7.4) to a total volume of 10.0 mL. To determine the drug loading amount, an aliquot of paclitaxel-loaded micellar solution was lyophilized and then dissolved in CH_3CN. The loading content (LC) was calculated according to the equation LC = $[W_{loaded}]/[W_{polymer} + W_{loaded}] \times 100\%$, where W_{loaded} and $W_{polymer}$ refer to the weights of drug encapsulated by micelles and total diblock copolymers, respectively.[63] Thus, the paclitaxel loading content was calculated to be ~5.0 wt/wt% based on the UV absorbance of paclitaxel at 228 nm against a standard calibration curve.

In vitro drug release measurements

Typically, 2.5 mL paclitaxel-loaded mixed micellar solution (1.0 g L^{-1}) of PCL-*b*-P(OEGMA-Gd) and PCL-*b*-P(OEGMA-FA) (1 : 1, wt/wt) in PBS (0.02 M, pH 7.4) were placed in a dialysis tube (cellulose membrane; MWCO is 3,500 Da) and then

immersed into 250 mL PBS medium under gentle stirring at 37 °C. Periodically, 20 mL external buffer solution was removed and replaced with equal volume of fresh buffer medium. Upon each sampling, 20 mL buffer solution was lyophilized. The paclitaxel concentration was then quantified by HPLC measurements.

In vitro cytotoxicity assay

Folate receptor over-expressing HeLa cells were employed for *in vitro* cytotoxicity evaluation *via* the MTT assay. HeLa cells were first cultured in Dulbecco's modified Eagle medium (DMEM) supplemented with 10% fetal bovine serum (FBS), penicillin (100 units mL^{-1}), and streptomycin (100 mg L^{-1}) at 37 °C in a CO_2–air (5 : 95) incubator for 2 days. For the cytotoxicity assay, HeLa cells were seeded in a 96-well plate at an initial density of *ca.* 5000 cells/well in 100 μL of complete DMEM medium. After incubating for 24 h, DMEM was replaced with fresh medium, and the cells were treated with micellar solution at varying final concentrations. The treated cells were incubated in a humidified environment with 5% CO_2 at 37 °C for 48 h. The MTT reagent (in 20 μL PBS, 5.0 g L^{-1}) was added to each well. The cells were further incubated for 4 h at 37 °C. The medium in each well was then removed and replaced by 150 μL DMSO. The plate was gently agitated for 15 min before the absorbance at 570 nm was recorded by a microplate reader (Thermo Fisher). Each experiment was conducted in quadruple and the data are shown as the mean value plus a standard deviation (± SD).

In vitro MR relaxivity measurements

The longitudinal relaxation rates ($1/T_1$) of the mixed micelles of PCL-*b*-P(OEGMA-Gd) and PCL-*b*-P(OEGMA-FA) (1 : 1, wt/wt) and a small molecule contrast agent, alkynyl-DOTA-Gd, in aqueous solution at varying Gd^{3+} concentrations (0, 0.04, 0.08, 0.16, and 0.50 mM) were acquired at room temperature using a GE Signa Horizon 1.5 T MR scanner equipped with a human shoulder coil. A conventional spin-echo pulse sequence was used for T_1 measurements with a single slice thickness of 4 mm, field of view (FOV) of 10 × 10 cm, and matrix size of 128 × 128. The repetition times (TR) were 300, 400, 500, 600, 800, 1000, 2000, and 3000 ms with an echo time (TE) of 9 ms. The net magnetizations for each sample were determined from the selected region of interest (ROI) and fit to the following multiparametric nonlinear regression function: $M_{TR} = M_0\,(1 - e^{-TR/T1})$, where M_{TR} denotes the measured signal intensity as a functional of repetition time (TR) and M_0 is the signal intensity in the thermal equilibrium. T_1 values were calculated from these data using a MATLAB program and the longitudinal relaxivity r_1 was determined from the slope of a $1/T_1$ *versus* [Gd^{3+}] plot.

In vitro MR imaging of HeLa cells

Folate receptor over-expressing HeLa cells were first cultured in DMEM supplemented with 10% FBS, penicillin (100 units mL^{-1}), and streptomycin (100 μg mL^{-1}) at 37 °C in a CO_2–air (5 : 95) incubator for 2 days. Then HeLa cells were seeded in a 24-well plate at an initial density of *ca.* 150 000 cells/well in 1.0 mL complete DMEM medium. After incubating for 24 h, the cells were treated with FA-free mixed micelles of PCL-*b*-P(OEGMA-Gd) and PCL-*b*-P(OEGMA-*co*-AzPMA) (1 : 1, wt/wt), and FA-labeled mixed micelles of PCL-*b*-P(OEGMA-Gd) and PCL-*b*-P(OEGMA-FA) (1 : 1, wt/wt), respectively. After 4 h, the culture media were removed and cells were washed, trypsinized, and neutralized. After centrifugation at 1000 rpm for 5 min, cells were re-suspended in 0.6 mL of PBS and 0.6 mL of 2.0 wt/v% paraformaldehyde, followed by incubation at 4 °C for 1 h. Then cells were washed with PBS to remove paraformaldehyde and centrifuged at 1000 rpm for 5 min. 0.5 mL fresh PBS was added together with 0.5 mL 2.0 wt/v% agarose solution onto cells. The mixture was then transferred into a 1.5 mL centrifuge tube. Cells were kept at 4 °C overnight before MRI scan. Images were obtained on a GE Signa Horizon 1.5 T MR scanner in a human shoulder coil using the Axial 3D FGRE sequence. The MRI intensity was compared to the untreated control, *i.e.*, the mixture of HeLa cells, PBS, and agarose gel.

In vivo MR imaging

All experiments concerning live animals were performed in accordance with the guidelines issued by the Ethical Committee of University of Science and Technology of China.

Normal male New Zealand rabbits (2.0 Kg) were employed for the *in vivo* examination of small animals by MR imaging. The rabbits were first anesthetized by the intravenous injection of ketamine (80 mg kg^{-1}) and xylazine (12 mg kg^{-1}). Contrast-enhanced images of rabbits were obtained on a GE Signa Horizon 1.5 T MR scanner in a human shoulder coil using the Axial 3D FGRE sequence. The imaging parameters chosen were TE = 9 ms, TR = 600 ms, 25 flip angle, 3D acquisition with 64 slices/slab, 120 mm FOV, and 0.5 mm coronal slice thickness. Each data set possesses an acquisition time of 2 min. The polymeric contrast agents were injected at a dose of 0.16 mmol Gd^{3+} kg^{-1} *via* the ear vein into the anaesthetized rabbit. Images were acquired at pre-injection and at 5, 10, 15, 30, 60, 90, and 120 min post-injection of the contrast agents. The effects of contrast enhancement by mixed micelles of PCL-*b*-P(OEGMA-Gd) and PCL-*b*-P(OEGMA-FA) (1 : 1, wt/wt) were investigated in a group of three rabbits. The time-dependent changes in normalized signal intensities were calculated by S_p/S_m, where S_p and S_m denote the signal intensity in the region of interest (ROI) post-injection and pre-injection, respectively.

Characterization

All nuclear magnetic resonance (NMR) spectra were recorded on a Bruker AV300 NMR 300 MHz spectrometer operated in the Fourier transform mode. $CDCl_3$ and DMSO-d_6 were used as the solvents. Molecular weights and molecular weight distributions were determined by gel permeation chromatography (GPC) equipped with a Waters 1515 pump and a Waters 2414 differential refractive index detector (set at 30 °C). It used a series of two linear Styragel columns (HR2 and HR4) at an oven temperature of 45 °C. The eluent was THF at a flow rate of 1.0 mL min^{-1}. A series of low polydispersity polystyrene standards were employed for calibration. Fourier transform infrared (FT–IR) spectra were recorded on a Bruker VECTOR-22 IR spectrometer. The spectra were collected over 64 scans with a spectral resolution of 4 cm^{-1}. Inductively coupled plasma atomic

emission spectrometry (ICP–AES) (Perkin Elmer Corporation Optima 7300 DV) was used for Gd(III) content analysis. The concentration of paclitaxel during drug release profile measurements was determined by an isocratic reverse-phase HPLC (LC-20AD Series, Shimadzu Corporation, Kyoto, Japan) at 25 °C. The mobile phase consisted of acetonitrile–water (45 : 55 v/v) at a flow rate of 1.0 mL min^{-1} and the wavelength of the ultraviolet detector was set at 228 nm. Dynamic laser light scattering (LLS) measurements were conducted on a commercial spectrometer (ALV/DLS/SLS-5022F) equipped with a multi-tau digital time correlator (ALV5000) and a cylindrical 22 mW UNIPHASE He–Ne laser (λ_0 = 632 nm) as the light source. Scattered light was collected at a fixed angle of 90° for a duration of ~5 min. Distribution averages and particle size distributions were computed using cumulants analysis and CONTIN routines. All data were averaged over three measurements. All samples were filtered through 0.45 μm Millipore Acrodisc-12 filters to remove dust. Transmission electron microscopy (TEM) observations were conducted on a Hitachi H-800 electron microscope at an acceleration voltage of 200 kV. AFM measurements were performed on a Digital instrument Multimode Nanoscope IIID operating in the tapping mode under ambient conditions. A silicon cantilever (RFESP) with a resonance frequency of ~80 kHz and a spring constant of ~3 N m^{-1} was used. The setpoint amplitude ratio was maintained at 0.7 to minimize sample deformation induced by the tip.

3. Results and discussion

Synthesis and co-micellization of PCL-*b*-P(OEGMA-FA) and PCL-*b*-P(OEGMA-Gd) amphiphilic diblock copolymers

Amphiphilic diblock copolymers, PCL-*b*-P(OEGMA-FA) and PCL-*b*-P(OEGMA-Gd), were synthesized *via* the combination of ATRP, ROP, and subsequent "click" functionalization (Scheme 2). The hydroxyl-terminated water-soluble P(OEGMA-*co*-AzPMA) ROP macroinitiator was synthesized at first *via* the ATRP of OEGMA and AzPMA by using HBMP as the initiator. GPC analysis revealed an M_n of 8000 and a M_w/M_n of 1.13 (Fig. 1a). The co-monomer molar contents in the copolymer were estimated from the monomer conversion as determined from ^{1}H NMR analysis of the reaction mixture before purification. The obtained $P(OEGMA_{0.83}\text{-}co\text{-}AzPMA_{0.17})_{18}$ precursor was employed as the initiator for the ROP of CL in anhydrous toluene at 70 °C, affording PCL-*b*-P(OEGMA-*co*-AzPMA) amphiphilic diblock copolymer bearing azide moieties in the hydrophilic POEGMA diblock. A typical GPC trace of PCL-*b*-P(OEGMA-*co*-AzPMA) shown in Fig. 1b revealed a monomodal elution peak and a clear shift to the higher molecular weight (MW) side compared to the P(OEGMA-*co*-AzPMA) precursor, indicating an almost quantitative initiating efficiency of P(OEGMA-*co*-AzPMA) macroinitiator. The actual DP of the PCL block was determined to be 64 by ^{1}H NMR from the signal integration ratio of peak a (methylene protons adjacent to carbonyl) and peak p (methylene protons adjacent to ester functionality) (see Fig. S1a, ESI†). The presence of azide moieties in PCL-*b*-P(OEGMA-*co*-AzPMA) can be clearly verified by the characteristic infrared absorption peak at ~2100 cm^{-1} (Fig. S2c†).

The copper(I)-catalyzed alkyne–azide click reaction has been broadly employed for the synthesis of various functionalized polymers with varying chain topologies due to its high efficiency. In the current work, this well-established reaction was employed for the synthesis of PCL-*b*-P(OEGMA-FA) and PCL-*b*-P(OEGMA-Gd) amphiphilic diblock copolymers. For the synthesis of PCL-*b*-P(OEGMA-FA), PCL-*b*-P(OEGMA-*co*-AzPMA) was reacted with an excess of alkynyl-folate in the presence of CuBr–PMDETA catalyst in DMF to ensure the complete transformation of the azide moieties for the efficient grafting of FA targeting functionalities onto the hydrophilic POEGMA block. The ^{1}H NMR spectrum of PCL-*b*-P(OEGMA-FA) is shown in Fig. S1b†, together with the peak assignments. The appearance of new signals characteristic of folate moieties in the range of 6.5–8.7 ppm confirmed the successful functionalization of FA moieties. The FT–IR spectra shown in Fig. S2† further verified the quantitative azide group transformation and the complete removal of unreacted alkynyl-folate by the disappearance of the characteristic infrared absorption peaks of both the azide moieties at ~2100 cm^{-1} and the alkynyl functionalities at ~2120 cm^{-1}. In addition, GPC analysis of PCL-*b*-P(OEGMA-FA) revealed a slight shift to the higher MW side compared to that of PCL-*b*-P(OEGMA-*co*-AzPMA) (Fig. 1d). By employing similar procedures, the PCL-*b*-P(OEGMA-Gd) diblock copolymer was also synthesized (Fig. 1c and Fig. S2d†). The Gd^{3+} content within the amphiphilic diblock copolymer was determined to be ~2.8 wt% by ICP–AES measurements.

In the current work, cancer cell-targeted mixed micelles were prepared *via* the co-assembly of PCL-*b*-P(OEGMA-FA) and PCL-*b*-P(OEGMA-Gd) (1 : 1, wt/wt) in water. The mixed micelles were then characterized by dynamic LLS, TEM, and AFM. For comparison, two other types of micelles were also prepared *via* the micellization of PCL-*b*-P(OEGMA-FA) and PCL-*b*-P(OEGMA-Gd) diblock copolymers, respectively.

As revealed by dynamic LLS in Fig. 2a, the aqueous micellar solution of PCL-*b*-P(OEGMA-Gd) exhibits an intensity-average hydrodynamic radius, $<R_h>$, of 23.6 nm. Similarly, the aqueous micellar solution of PCL-*b*-P(OEGMA-FA) exhibits an $<R_h>$ of 38.3 nm (Fig. 2b). The slightly larger $<R_h>$ of the latter is presumably due to the partial hydrophobicity of FA moieties within the P(OEGMA-*co*-*FA*) block, whereas the DOTA-Gd complex is more hydrophilic. On the other hand, dynamic LLS

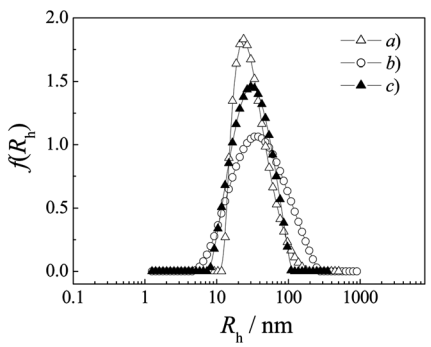

Fig. 2 Hydrodynamic radius distributions, $f(R_h)$, recorded for a 0.5 g L^{-1} aqueous micellar solution of (a) PCL-*b*-P(OEGMA-Gd), (b) PCL-*b*-P(OEGMA-FA), and (c) PCL-*b*-P(OEGMA-Gd) and PCL-*b*-P(OEGMA-FA) (1 : 1, wt/wt).

revealed an $<R_h>$ of 27.8 nm and a μ_2/Γ^2 of 0.151 for mixed micelles co-assembled from PCL-*b*-P(OEGMA-FA) and PCL-*b*-P(OEGMA-Gd) diblock copolymers (1 : 1, wt/wt). In addition, the mixed micelles possess an apparent molar mass, $M_{w,app}$, of 3.3×10^6 g mol^{-1}. Thus, we can calculate that on average, each mixed micelle contains ~199 FA moieties and ~199 DOTA-Gd functionalities, respectively. A typical TEM image obtained by drying the aqueous solution of mixed micelles revealed the presence of fairly monodisperse and mostly spherical nanoparticles with a diameter of ~40 nm (Fig. 3a), which is in reasonable agreement with that determined by dynamic LLS (Fig. 2). It is well known that the TEM technique determines nanoparticle dimensions in the dry state, whereas dynamic LLS reports intensity-average dimensions in solution. The spherical morphology of the micellar nanoparticles was further confirmed by AFM measurements (Fig. 3b). Moreover, the stability of the mixed micelles in water, PBS (0.02 M, pH 7.4), and PBS with 10% fetal bovine serum against extended storage duration was also examined by LLS (Fig. S3, ESI†), which suggested that mixed micelles possessing highly hydrophilic brush-like POEGMA coronas are stable over a period of ~100 h.

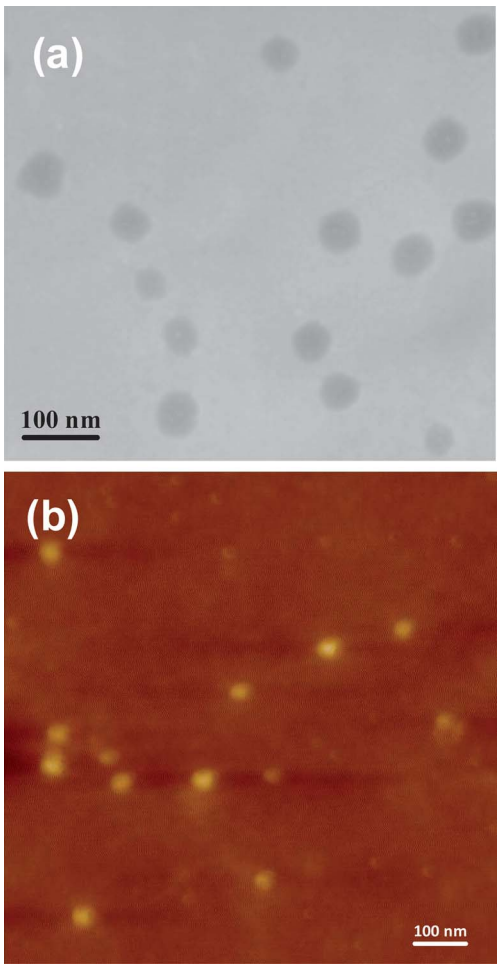

Fig. 3 Typical (a) TEM and (b) AFM images recorded for mixed micelles of PCL-*b*-P(OEGMA-Gd) and PCL-*b*-P(OEGMA-FA) (1 : 1, wt/wt).

***In vitro* drug release and cell viability evaluation.** A well-known hydrophobic anticancer drug, paclitaxel, was physically encapsulated within the inner hydrophobic core of mixed micelles.[64–66] The drug loading content of the mixed micelles was determined to be ~5.0 wt/wt%. Subsequently, the *in vitro* drug release characteristics of paclitaxel-loaded mixed micelles were examined under simulated physiological conditions (PBS, pH 7.4, 37 °C). As shown in Fig. 4, an almost linear release of the encapsulated drug can be observed in the first 15 h, resulting in a ~30% cumulative drug release in this time period. This indicates that these novel types of mixed micelles are good candidates as controlled release drug nanocarriers. At extended time periods, the release rate slows down and the cumulative drug release reaches ~60% after 130 h.

Aiming to explore the *in vitro* anticancer efficacy, HeLa cells were employed to evaluate the cytotoxicity of paclitaxel-loaded mixed micelles using the standard MTT assay. As shown in Fig. 5a, drug-free mixed micelles of PCL-*b*-P(OEGMA-FA) and PCL-*b*-P(OEGMA-Gd) (1 : 1, wt/wt) exhibit negligible cytotoxicity with >80% cell viability at a micellar concentration of up to 0.2 g L^{-1}. This is in accordance with the well-recognized biocompatibility of PEG and PCL segments. However, by treating HeLa cells with paclitaxel-loaded mixed micelles, considerably decreased cell viability was observed, with ~28.3% of HeLa cells remaining alive at a micellar concentration of 0.2 g L^{-1} (the loaded paclitaxel concentration is 10 mg L^{-1}). It is worthy of note that in the current study, cancer cell-targeting FA moieties were anchored within the corona layer rather than at the terminal periphery of mixed micelles. Considering their potential *in vivo* applications, the hydrophilic and generally inert POEGMA coronas are expected to effectively protect FA moieties from undesirable enzymatic attack and premature endocytosis processes during the blood circulation period.

In vitro MR imaging contrast enhancement by mixed polymeric micelles

In this section, the MR imaging contrast enhancement performances of mixed micelles co-assembled from PCL-*b*-P(OEGMA-FA) and PCL-*b*-P(OEGMA-Gd) (1 : 1, wt/wt) were probed. It has been well documented that small molecular Gd^{3+}-based T_1-type MR imaging contrast agents often suffer from limited sensitivity and unsatisfactory life span in the human body, which greatly impair their further development in clinical

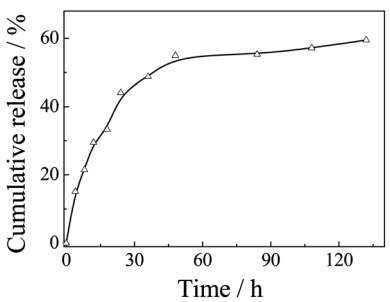

Fig. 4 *In vitro* drug release profile of paclitaxel from drug-loaded mixed micelles of PCL-*b*-P(OEGMA-Gd) and PCL-*b*-P(OEGMA-FA) (1 : 1, wt/wt) at 37 °C (phosphate buffer; 0.02 M, pH 7.4).

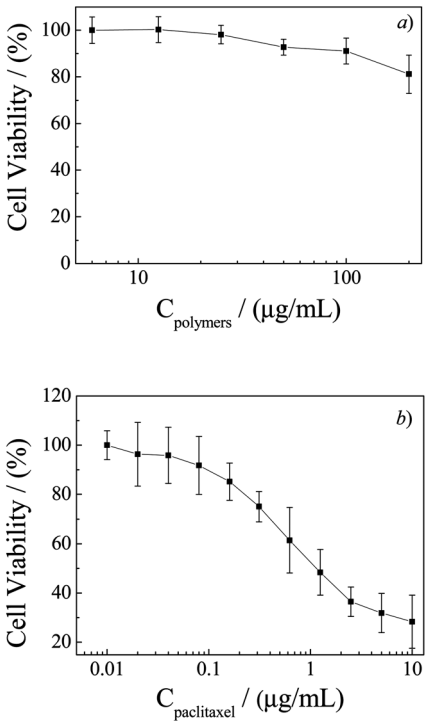

Fig. 5 (a) *In vitro* cytotoxicity of mixed micelles of PCL-*b*-P(OEGMA-Gd) and PCL-*b*-P(OEGMA-FA) (1 : 1, wt/wt) determined by a MTT assay against HeLa cells. (b) Viability of HeLa cells incubated for 48 h with paclitaxel-loaded mixed micelles of PCL-*b*-P(OEGMA-Gd) and PCL-*b*-P(OEGMA-FA) (1 : 1, wt/wt) in aqueous solution at varying paclitaxel concentrations.

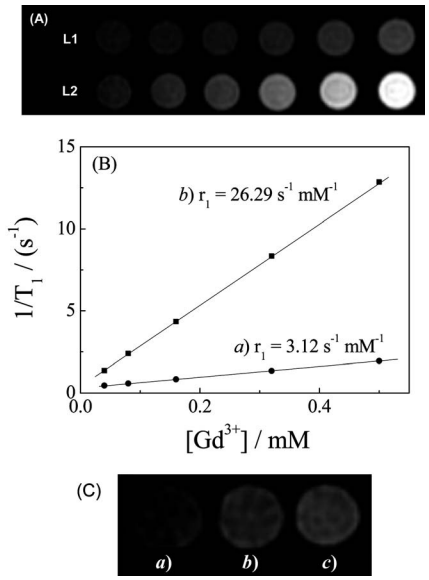

Fig. 6 (A) T_1 weighted spin-echo MR images of (L1) alkynyl-DOTA-Gd and (L2) mixed micelles of PCL-*b*-P(OEGMA-Gd) and PCL-*b*-P(OEGMA-FA) (1 : 1, wt/wt) in water with Gd^{3+} concentrations being 0, 0.04, 0.08, 0.16, 0.32, and 0.50 mM (from left to right), respectively. Images were obtained at 1.5 T (TR/TE = 600/9 ms) at room temperature. (B) The water proton longitudinal relaxation rate ($1/T_1$) of (a) alkynyl-DOTA-Gd and (b) mixed micelles of PCL-*b*-P(OEGMA-Gd) and PCL-*b*-P(OEGMA-FA) (1 : 1, wt/wt) in aqueous solution as a function of Gd^{3+} concentration. (C) MR images recorded for (a) untreated HeLa cells, and HeLa cells treated with (b) 0.2 g L^{-1} FA-free mixed micelles of PCL-*b*-P(OEGMA-Gd) and PCL-*b*-P(OEGMA-*co*-AzPMA) (1 : 1, wt/wt), and (c) 0.2 g L^{-1} FA-decorated mixed micelles of PCL-*b*-P(OEGMA-Gd) and PCL-*b*-P(OEGMA-FA) (1 : 1, wt/wt), respectively.

applications. Various strategies have been developed to improve their contrast enhancement performances.[19,52–55,57] In the current work, we fabricated a novel type of cancer cell-targeted mixed polymeric micelles as a nanoplatform to increase the T_1 relaxivity of MR imaging contrast agents and prolong the blood circulation time. In an effort to improve the location specificity of MR imaging contrast agents, in the current work, the targeting moieties, folic acid, together with DOTA-Gd were covalently anchored into the hydrophilic POEGMA coronas of mixed micelles *via* the co-assembly approach.

Typical T_1 weighted spin-echo MR images recorded for mixed micelles of PCL-*b*-P(OEGMA-FA) and PCL-*b*-P(OEGMA-Gd) (1 : 1, wt/wt) at varying Gd^{3+} concentrations in water are shown in Fig. 6A. The performance of a small DOTA-Gd complex was measured at first as a control. Upon gradually increasing the concentration of alkynyl-DOTA-Gd, we can observe a clear positive contrast enhancement of MR signals as revealed by the reinforcement of spot brightness. Most importantly, the corresponding mixed micelle-based contrast agents in the same Gd^{3+} concentration range exhibit substantially enhanced MR signal contrast, confirming the well-documented fact that attaching multiple small molecule Gd^{3+} complexes into nanoassemblies, polymer scaffolds, and dendrimers can typically improve the signal contrast effects.

Quantitative analysis was further conducted to investigate the enhancement of the MR imaging performance (Fig. 6B). Data analysis based on Matlab software indicated a linear relationship between the water proton longitudinal relaxation rate ($1/T_1$) and the Gd^{3+} concentration. Small molecule alkynyl-DOTA-Gd possesses a relaxivity (r_1) of 3.12 s^{-1} mM^{-1}, which is in reasonable agreement with that reported for DOTA-Gd.[14,58] On the other hand, linear regression analysis of a $1/T_1$ *versus* [Gd^{3+}] plot for the mixed micellar solution revealed a substantially enhanced contrast efficiency, as evidenced by the much larger slope of the plot compared to that for alkynyl-DOTA-Gd. For the mixed micelles, the T_1 relaxivity (r_1) was calculated to be 26.29 s^{-1} mM^{-1}. Thus, a ~8.3-fold enhancement in comparison with that of alkynyl-DOTA-Gd was achieved. These positive results augur well for the application of mixed micelles as excellent T_1-type contrast agents integrated with targeted drug delivery and controlled release functions.

In order to investigate the differences in cellular uptake of FA-free and FA-labeled mixed micelles, MR images of wells containing folate-receptor overexpressing HeLa cells incubated with FA-free and FA-decorated mixed micelles were conducted. As shown in Fig. 6C, untreated cells exhibit relatively weak MR signal intensity. Whereas upon treating with the FA-free mixed micelles of PCL-*b*-P(OEGMA-Gd) and PCL-*b*-P(OEGMA-*co*-AzPMA), an enhanced positive contrast enhancement of MR signals can be observed, as revealed by the reinforcement of spot brightness. Quantitative analysis revealed that the signal intensity increased by approximately 55.5%. Concomitantly, upon treating with the FA-decorated mixed micelles of

PCL-*b*-P(OEGMA-Gd) and PCL-*b*-P(OEGMA-FA), the MR signal intensity exhibited a ~84.1% enhancement compared to the control, indicating the presence of specific folate-receptor mediated endocytosis events, in addition to the non-specific one.

In vivo time-dependent MR imaging assessment of mixed polymeric micelles

The fast clearance of small molecule chemotherapeutic drugs or MR imaging contrast agents and their poor accumulation within tumor sites are major concerns associated with *in vivo* cancer chemotherapy and diagnostic MR imaging examinations.[1,19] Thus, nanocarriers or theranostic nanomedicines with extended blood circulation duration and preferential accumulation within tumor sites are highly desirable.[7,8] In the current work, the POEGMA hydrophilic corona of mixed micelles is expected to protect micellar nanocarriers from non-specific interactions with serum components during blood circulation. To evaluate the *in vivo* MR imaging contrast performance of mixed micelles, we measured time-dependent changes of MR imaging signal intensities by using white rabbits as the animal model. As shown in Fig. 7, typical rabbit liver slices exhibit a relatively dark background before the administration of mixed micelle-based MR imaging contrast agents. At 10 min post-injection a substantial increase in brightness of the liver region can be discerned. At 30 min post-injection, the brightness further increased and the maximum signal intensity was reached. The time period of relatively high resolution and brightness can be maintained up to ~60 min. After that, the signal intensity considerably decreases, and ~120 min post-injection, the signal intensity restores to the value comparable to that at pre-injection.

In an effort to further probe the performance of mixed micelle-based MR imaging contrast agents and compare them with those of the small molecule Gd complex and the FA-free mixed micelles, quantitative analysis was then conducted (Fig. 8). Small molecule alkynyl-DOTA-Gd, non-targeting mixed micelles co-assembled from PCL-*b*-P(OEGMA-*AzPMA*) and PCL-*b*-P(OEGMA-Gd) (1 : 1, wt/wt), and cancer cell-targeting polymeric micelles co-assembled from PCL-*b*-P(OEGMA-FA) and PCL-*b*-P(OEGMA-Gd) (1 : 1, wt/wt) were intravenously administered into white rabbits at a dose of 0.16 mmol Gd^{3+} kg^{-1} body weight, respectively. As depicted in Fig. 8a, upon injection of small molecule alkynyl-DOTA-Gd, the normalized MR signal intensity increased rapidly and reached the maximum intensity value of 1.36 at 5.4 min post-injection. After ~20 min post-injection, the signal intensity decayed to the background value.

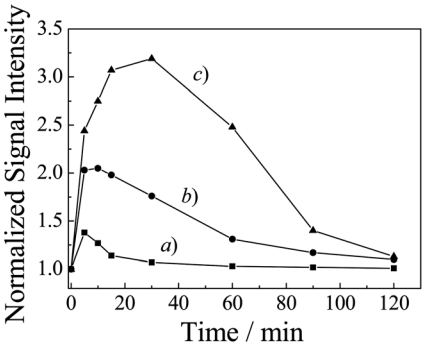

Fig. 8 The time evolution of normalized signal intensity recorded in the rabbit liver at pre-injection and 5, 10, 15, 30, 60, 90, and 120 min after intravenous injection of (a) alkynyl-DOTA-Gd, (b) mixed micelles of PCL-*b*-P(OEGMA-Gd) and PCL-*b*-P(OEGMA-*co*-AzPMA) (1 : 1, wt/wt), and (c) mixed micelles of PCL-*b*-P(OEGMA-Gd) and PCL-*b*-P(OEGMA-FA) (1 : 1, wt/wt), respectively at a dose of 0.16 mmol Gd^{3+} kg^{-1}.

On the contrary, FA-labeled mixed micelles exhibit dramatically enhanced signal intensity and prolonged residence time. As shown in Fig. 8c, the relative signal intensity reached the maximum value of 3.19 at 30 min post-injection. Upon administration of FA-labeled mixed micelles, the contrast enhancement can last ~92 min while still maintaining a better contrast performance (>1.36) than that exhibited by the small molecule Gd complex (the maximum relative intensity value is 1.36). The enhanced MR imaging resolution and prolonged retention and circulation duration of the FA-labeled mixed micelles imply that they are suitable for more accurate medical diagnosis, integration with other detection modalities, and *in situ* monitoring of

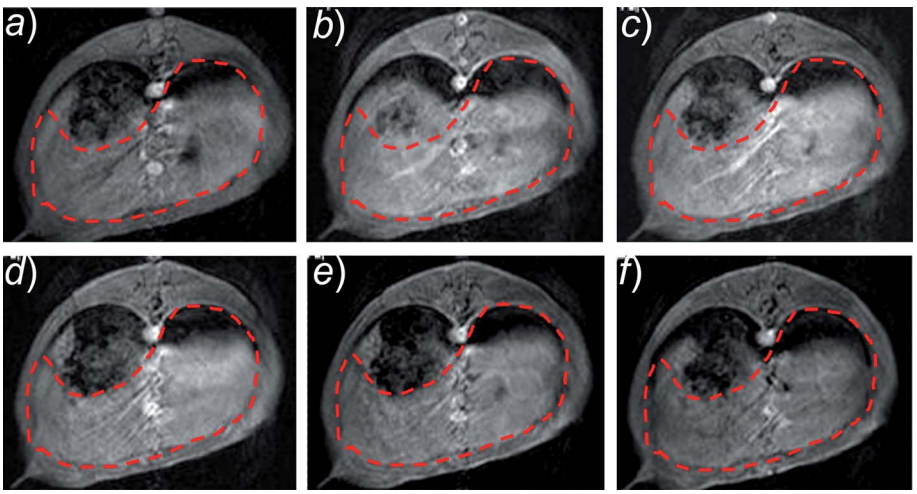

Fig. 7 MR images recorded for liver slices of rabbits at (a) pre-injection, (b) 10, (c) 30, (d) 60, (e) 90, and (f) 120 min after intravenous injection of a mixed micellar solution of PCL-*b*-P(OEGMA-Gd) and PCL-*b*-P(OEGMA-FA) (1 : 1, wt/wt) at a dose of 0.16 mmol Gd^{3+} kg^{-1}.

pharmacokinetic processes and biodistribution of drug-loaded nanocarriers. To further investigate the role of the targeting moieties (FA) in the mixed micelles co-assembled from PCL-*b*-P(OEGMA-FA) and PCL-*b*-P(OEGMA-Gd) (1 : 1, wt/wt), we also probed the MR imaging contrast performance of FA-free mixed micelles, and the results are plotted in Fig. 8b. It was found that although the non-targeted mixed micelle-based contrast agents (reaching the highest relative signal intensity, 2.05, at ~10 min post-injection) outperformed the small molecule alkynyl-DOTA-Gd complex, the overall contrast enhancement performance was not as good as that of the FA-labeled mixed micelles (Fig. 8c). These results indicated that the FA targeting moieties play an indispensible role in enhancing accumulation and retention of the mixed micellar nanoparticles within the rabbit liver organ, although in the current work a healthy rabbit model without transplantation of a tumor xenograft was used as the animal model.

4. Conclusions

In summary, mixed polymeric micelles co-assembled from PCL-*b*-P(OEGMA-Gd) and PCL-*b*-P(OEGMA-FA) amphiphilic diblock copolymers were utilized as a new type of nanoplatform for synergistic cancer cell-targeted delivery of anticancer drugs and MR imaging contrast enhancement. The mixed micelles possess hydrophobic PCL cores for the physical encapsulation of a hydrophobic chemotherapeutic drug (paclitaxel) and hydrophilic hybrid POEGMA coronas covalently labeled with DOTA-Gd complex and folic acid (FA) moieties for MR imaging contrast enhancement and tumor targeting functions, respectively. Paclitaxel-loaded mixed micelles exhibit controlled-release characteristics, *i.e.*, ~60% loaded drugs were released over a time duration of ~130 h. *In vitro* MR imaging characterization reveals that the T_1 relaxivity of mixed micelles ($r_1 = 26.29\ s^{-1}\ mM^{-1}$) is ~8.3-fold higher than that of the small molecule alkynyl-DOTA-Gd complex ($3.12\ s^{-1}\ mM^{-1}$). In addition, *in vivo* MR imaging tests in rabbits exhibit considerably enhanced MR signal intensity, prominent positive contrast enhancement, improved accumulation, and extended duration of blood circulation for FA-labeled mixed micellar nanoparticles within the rabbit liver in comparison with that of FA-free mixed micelles and a small molecule alkynyl-DOTA-Gd complex.

Acknowledgements

The financial support from National Natural Scientific Foundation of China (NNSFC) Project (51033005, 20874092, and 91027026) and Fundamental Research Funds for the Central Universities is gratefully acknowledged.

References

1 C. Oerlemans, W. Bult, M. Bos, G. Storm, J. F. W. Nijsen and W. E. Hennink, *Pharm. Res.*, 2010, **27**, 2569–2589.
2 T. Lammers, V. Subr, K. Ulbrich, W. E. Hennink, G. Storm and F. Kiessling, *Nano Today*, 2010, **5**, 197–212.
3 R. Duncan, *Nat. Rev. Drug Discovery*, 2003, **2**, 347–360.
4 D. Sutton, N. Nasongkla, E. Blanco and J. M. Gao, *Pharm. Res.*, 2007, **24**, 1029–1046.
5 M. L. Adams, A. Lavasanifar and G. S. Kwon, *J. Pharm. Sci.*, 2003, **92**, 1343–1355.
6 A. B. E. Attia, Z. Y. Ong, J. L. Hedrick, P. P. Lee, P. L. R. Ee, P. T. Hammond and Y. Y. Yang, *Curr. Opin. Colloid Interface Sci.*, 2011, **16**, 182–194.
7 J. R. McCarthy, *Nanomedicine*, 2009, **4**, 693–395.
8 J. M. Gao and B. Sumer, *Nanomedicine*, 2008, **3**, 137–140.
9 X. W. Ma, Y. L. Zhao and X. J. Liang, *Acc. Chem. Res.*, 2011, **44**, 1114–1122.
10 J. E. Lee, N. Lee, T. Kim, J. Kim and T. Hyeon, *Acc. Chem. Res.*, 2011, **44**, 893–902.
11 S. S. Kelkar and T. M. Reineke, *Bioconjugate Chem.*, 2011, **22**, 1879–1903.
12 D. Ho, X. L. Sun and S. H. Sun, *Acc. Chem. Res.*, 2011, **44**, 875–882.
13 M. E. Caldorera-Moore, W. B. Liechty and N. A. Peppas, *Acc. Chem. Res.*, 2011, **44**, 1061–1070.
14 J. A. Barreto, W. O'Malley, M. Kubeil, B. Graham, H. Stephan and L. Spiccia, *Adv. Mater.*, 2011, **23**, H18–H40.
15 S. M. Janib, A. S. Moses and J. A. MacKay, *Adv. Drug Delivery Rev.*, 2010, **62**, 1052–1063.
16 M. E. Davis, Z. Chen and D. M. Shin, *Nat. Rev. Drug Discovery*, 2008, **7**, 771–782.
17 Z. R. Lu, F. Ye and A. Vaidya, *J. Controlled Release*, 2007, **122**, 269–277.
18 S. Aime, E. Terreno, D. D. Castelli and A. Viale, *Chem. Rev.*, 2010, **110**, 3019–3042.
19 M. W. Brechbiel, A. J. L. Villaraza and A. Bumb, *Chem. Rev.*, 2010, **110**, 2921–2959.
20 P. Hermann, J. Kotek, V. Kubicek and I. Lukes, *Dalton Trans.*, 2008, 3027–3047.
21 A. M. Raitsimring, C. Gunanathan, A. Potapov, I. Efremenko, J. M. L. Martin, D. Goldfarb and D. Milstein, *J. Am. Chem. Soc.*, 2007, **129**, 14138–14139.
22 S. Aime, M. Botta, F. Fedeli, E. Gianolio, E. Terreno and P. Anelli, *Chem.–Eur. J.*, 2001, **7**, 5262–5269.
23 R. Z. Xu, Y. L. Wang, X. L. Wang, E. K. Jeong, D. L. Parker and Z. R. Lu, *Exp. Biol. Med.*, 2007, **232**, 1081–1089.
24 Q. Zheng, H. Q. Dai, M. E. Merritt, C. Malloy, C. Y. Pan and W. H. Li, *J. Am. Chem. Soc.*, 2005, **127**, 16178–16188.
25 G. L. Liang, J. Ronald, Y. X. Chen, D. J. Ye, P. Pandit, M. L. Ma, B. Rutt and J. H. Rao, *Angew. Chem., Int. Ed.*, 2011, **50**, 6283–6286.
26 J. A. Peters, D. T. Schuhle, P. van Rijn, S. Laurent, L. Vander Elst, R. N. Muller, M. C. A. Stuart and J. Schatze, *Chem. Commun.*, 2010, **46**, 4399–4401.
27 B. von Rechenberg, T. Neuberger, B. Schopf, H. Hofmann and M. Hofmann, *J. Magn. Magn. Mater.*, 2005, **293**, 483–496.
28 Q. Gan, X. Y. Lu, Y. Yuan, J. C. Qian, H. J. Zhou, X. Lu, J. L. Shi and C. S. Liu, *Biomaterials*, 2011, **32**, 1932–1942.
29 H. M. Yang, H. J. Lee, K. S. Jang, C. W. Park, H. W. Yang, W. Do Heo and J. D. Kim, *J. Mater. Chem.*, 2009, **19**, 4566–4574.
30 P. Zou, Y. K. Yu, Y. A. Wang, Y. Q. Zhong, A. Welton, C. Galban, S. M. Wang and D. X. Sun, *Mol. Pharmaceutics*, 2010, **7**, 1974–1984.
31 R. M. Xing, X. Y. Wang, C. L. Zhang, J. Z. Wang, Y. M. Zhang, Y. Song and Z. J. Guo, *J. Mater. Chem.*, 2011, **21**, 11142–11149.
32 X. Q. Yang, J. J. Grailer, I. J. Rowland, A. Javadi, S. A. Hurley, D. A. Steeber and S. Q. Gong, *Biomaterials*, 2010, **31**, 9065–9073.
33 X. Q. Yang, J. J. Grailer, I. J. Rowland, A. Javadi, S. A. Hurley, V. Z. Matson, D. A. Steeber and S. Q. Gong, *ACS Nano*, 2010, **4**, 6805–6817.
34 J. Lee, J. Yang, H. Ko, S. J. Oh, J. Y. Kang, J. H. Son, K. Lee, S. W. Lee, H. G. Yoon, J. S. Suh, Y. M. Huh and S. J. Haam, *Adv. Funct. Mater.*, 2008, **18**, 258–264.
35 J. Yang, C. H. Lee, H. J. Ko, J. S. Suh, H. G. Yoon, K. Lee, Y. M. Huh and S. Haam, *Angew. Chem., Int. Ed.*, 2007, **46**, 8836–8839.
36 O. Veiseh, F. M. Kievit, C. Fang, N. Mu, S. Jana, M. C. Leung, H. Mok, R. G. Ellenbogen, J. O. Park and M. Q. Zhang, *Biomaterials*, 2010, **31**, 8032–8042.
37 J. M. Shin, R. M. Anisur, M. K. Ko, G. H. Im, J. H. Lee and I. S. Lee, *Angew. Chem., Int. Ed.*, 2009, **48**, 321–324.
38 A. Y. Louie, M. M. Huber, E. T. Ahrens, U. Rothbacher, R. Moats, R. E. Jacobs, S. E. Fraser and T. J. Meade, *Nat. Biotechnol.*, 2000, **18**, 321–325.
39 N. Kohler, C. Sun, J. Wang and M. Q. Zhang, *Langmuir*, 2005, **21**, 8858–8864.
40 J. Kim, Y. Piao and T. Hyeon, *Chem. Soc. Rev.*, 2009, **38**, 372–390.
41 C. Khemtong, C. W. Kessinger and J. M. Gao, *Chem. Commun.*, 2009, 3497–3510.

42 M. K. Yu, Y. Y. Jeong, J. Park, S. Park, J. W. Kim, J. J. Min, K. Kim and S. Jon, *Angew. Chem., Int. Ed.*, 2008, **47**, 5362–5365.
43 H. M. Yang, H. J. Lee, C. W. Park, S. R. Yoon, S. Lim, B. H. Jung and J. D. Kim, *Chem. Commun.*, 2011, **47**, 5322–5324.
44 H. Ai, C. Flask, B. Weinberg, X. T. Shuai, M. D. Pagel, D. Farrell, J. Duerk and J. M. Gao, *Adv. Mater.*, 2005, **17**, 1949–1952.
45 J. Lu, S. Ma, J. Sun, C. Xia, C. Liu, Z. Wang, X. Zhao, F. Gao, Q. Gong, B. Song, X. Shuai, H. Ai and Z. Gu, *Biomaterials*, 2009, **30**, 2919–2928.
46 J. H. Park, G. von Maltzahn, E. Ruoslahti, S. N. Bhatia and M. J. Sailor, *Angew. Chem., Int. Ed.*, 2008, **47**, 7284–7288.
47 J. S. Guthi, S. G. Yang, G. Huang, S. Li, C. Khemtong, C. W. Kessinger, M. Peyton, J. D. Minna, K. C. Brown and J. M. Gao, *Mol. Pharmaceutics*, 2009, **7**, 32–40.
48 A. Gianella, P. A. Jarzyna, V. Mani, S. Ramachandran, C. Calcagno, J. Tang, B. Kann, W. J. R. Dijk, V. L. Thijssen, A. W. Griffioen, G. Storm, Z. A. Fayad and W. J. M. Mulder, *ACS Nano*, 2011, **5**, 4422–4433.
49 N. Nasongkla, E. Bey, J. Ren, H. Ai, C. Khemtong, J. S. Guthi, S. F. Chin, A. D. Sherry, D. A. Boothman and J. M. Gao, *Nano Lett.*, 2006, **6**, 2427–2430.
50 D. Y. Chen, X. W. Xia, H. W. Gu, Q. F. Xu, J. F. Ge, Y. G. Li, N. J. Li and J. M. Lu, *J. Mater. Chem.*, 2011, **21**, 12682–12690.
51 J. Hu, Y. Qian, X. Wang, T. Liu and S. Liu, *Langmuir*, 2012, **28**, 2073–2082.
52 H. Y. Lee, H. W. Jee, S. M. Seo, B. K. Kwak, G. Khang and S. H. Cho, *Bioconjugate Chem.*, 2006, **17**, 700–706.
53 G. D. Zhang, R. Zhang, X. X. Wen, L. Li and C. Li, *Biomacromolecules*, 2008, **9**, 36–42.
54 K. Kono, S. Nakashima, D. Kokuryo, I. Aoki, H. Shimomoto, S. Aoshima, K. Maruyama, E. Yuba, C. Kojima, A. Harada and Y. Ishizaka, *Biomaterials*, 2011, **32**, 1387–1395.
55 K. Shiraishi, K. Kawano, T. Minowa, Y. Maitani and M. Yokoyama, *J. Controlled Release*, 2009, **136**, 14–20.
56 T. Liu, X. Li, Y. Qian, X. Hu and S. Liu, *Biomaterials*, 2012, **33**, 2521–2531.
57 J. L. Turner, D. Pan, R. Plummer, Z. Chen, A. K. Whittaker and K. L. Wooley, *Adv. Funct. Mater.*, 2005, **15**, 1248–1254.
58 X. J. Li, Y. F. Qian, T. Liu, X. Hu, G. Y. Zhang, Y. Z. You and S. Y. Liu, *Biomaterials*, 2011, **32**, 6595–6605.
59 H. Frey, F. F. Wolf and N. Friedemann, *Macromolecules*, 2009, **42**, 5622–5628.
60 B. S. Sumerlin, P. De and S. R. Gondi, *Biomacromolecules*, 2008, **9**, 1064–1070.
61 T. J. Meade, Y. Song and E. K. Kohlmeir, *J. Am. Chem. Soc.*, 2008, **130**, 6662–6663.
62 D. E. Prasuhn, R. M. Yeh, A. Obenaus, M. Manchester and M. G. Finn, *Chem. Commun.*, 2007, 1269–1271.
63 X. J. Wan, T. Liu and S. Y. Liu, *Biomacromolecules*, 2011, **12**, 1146–1154.
64 D. B. Yang, L. Yu and S. Van, *Cancers*, 2011, **3**, 17–42.
65 Y. Kataoka, N. Yagi, N. Kokubu, Y. Kasahara, M. Abe and Y. Otsuka, *Circ. J.*, 2011, **75**, 868–873.
66 K. Park, *J. Controlled Release*, 2010, **148**, 265–265.

